A New Planar Electromagnetic Levitation System Improvement Method Based on SIMLAB Platform in Real Time Operation

Mundher H. A. Yaseen[1, *] and Haider J. Abd[2]

Abstract—Electromagnetic levitation system is commonly used in the field of magnetic levitation system train. Magnetic levitation technology is one of the most promised issue of transportation and precision engineering. Magnetic levitation systems are free of problems caused by friction, wear, sealing and lubrication. In this paper, a new prototype of the magnetic levitation system is proposed, designed and successfully tested via SIMLAB platform in real time. In addition, the proposed system was implemented with an efficient controller, which is linear-quadratic regulator (LQR) and compared with a classical controller which is proportional-integral-derivative (PID). The present system has been tested with two different criteria: signal test and load test under different input signals which are Sine wave and Squar wave. The findings prove that the suggested levitation system reveals a better performance than conventional one. Moreover, the LQR controller produced a great stability and optimal response compared to PID controller used at same system parameters.

1. INTRODUCTION

Magnetic levitation technology is a perfect solution to achieve better performance for many motion systems, e.g., precision positioning, manipulation, suspension, and haptic interaction due to its non-contact, non-contamination, multi-Degrees-Of-Freedom (DOF), and long-stroke characteristics [1–4]. Recently, the research on magnetic levitation attracts many researchers, and various types of magnetically levitated (maglev) motion systems are proposed. Generally, these maglev motion systems are realized using either Lorentz force or electromagnetic force, and both the moving magnet design and moving-coil design are proposed for applications with different requirements.

In literature, different methods and models are suggested to develop electromagnetic levitation systems and improve the system response [5–17]. However, most of the contributions require data from measurement devices or observer algorithms. The position and electric current state data are taken from related measurement devices, but for velocity state data, an observer should be synthesized to estimate the unavailable signal of the nonlinear dynamical system. Furthermore, it needs a complex system design and is not cost efficient. In this paper, a new technique is proposed to develop the control system based on a plate maglev system with the mathematical model. The new system uses a SIMLAB platform to control the position of electromagnetically levitated system in real time via Matlab/Simulink environment.

2. MAGLEV SYSTEM CONSTRUCTION

In this section, firstly, the construction of the magnetic levitation system and its components will be explained.

* Corresponding author: Mundher H. A. Yaseen (mundheryaseen@gmail.com).

[1] Electrical & Electronics Engineering Department, Gaziantep University, Gaziantep, Turkey. [2] Department of Electrical Engineering, College of Engineering, Babylon University, Iraq.

Levitation system or maglev is a method by which an object is suspended with no support other than magnetic fields. Magnetic force is used to counteract the effects of the gravitational acceleration and any other acceleration. The two primary issues involved in magnetic levitation are lifting forces: providing an upward force sufficient to counteract gravity and stability: ensuring that the system does not spontaneously slide or flip into a configuration where the lift is neutralized. Maglev trains perform three different parts to operate in high speeds which are: Levitation, Propulsion and Guidance. This paper focus on the levitation system part.

The proposed experimental magnetic levitation system is shown in Figure 1. The system is made up 4 electromagnets as actuators for applying magnetic forces to achieve stable levitation and precise position control, a rigid square plate with 4 permanent magnets on each corner, and 4 Hall effect sensors for sensing the position of the levitating plate, and Va is coil applied voltage.
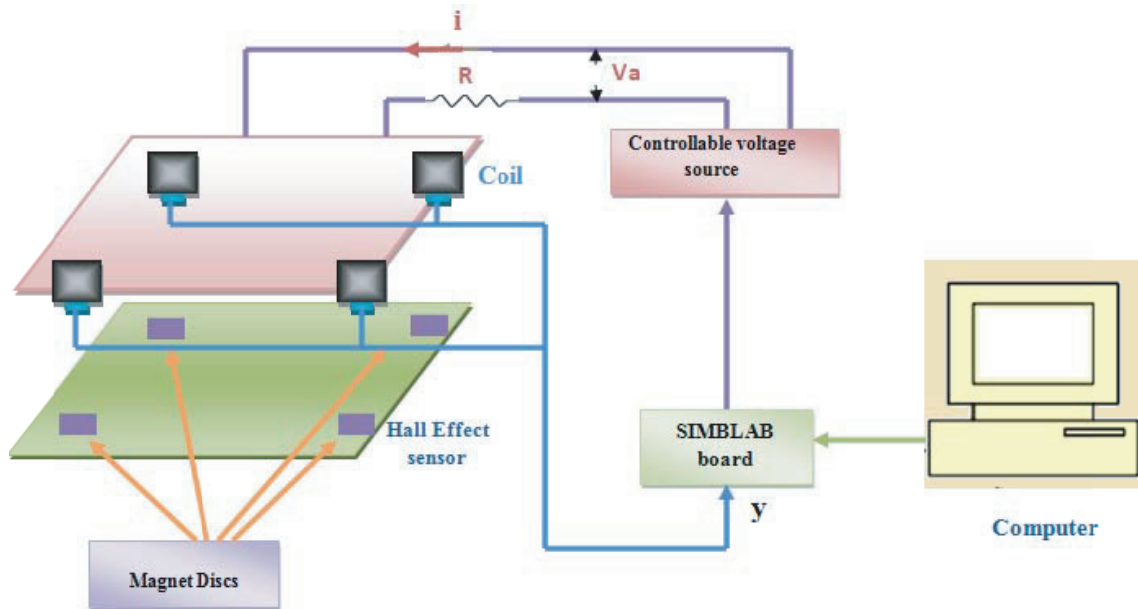

Figure 1. Free body diagram of magnetic levitation system.

The electromagnets are $15\,\text{mH}$ solenoid coils with $2\,\Omega$ internal resistances. The Hall effect sensors are linear ratiometric Hall effect sensors with $50\,\text{V/T}$. The permanent magnets are N52 neodymium disc magnets with $12.70\,\text{mm}$ diameter and $6.35\,\text{mm}$ thickness. The plate is a transparent acrylic plate with $152.4\,\text{mm} \times 152.4\,\text{mm} \times 3.175\,\text{mm}$. The frame is constructed by wood. For simplicity and tractability, the system is modeled using a quarter of the system (similar to a quarter car model). The model of the quarter-system is shown in Figure 2, where R is the resistance of the coil, L the inductance of the coil, v the voltage across the electromagnet, i the current through the electromagnet, m the mass of the levitating magnet plus one-forth of the mass of the acrylic plate, g the acceleration due to gravity, d the vertical position of the levitating magnet measured from the bottom of the electromagnet, F_{mag} the force on the levitating magnet generated by the electromagnet, and e the voltage across the Hall effect sensor.

3. CASE STUDY

In this section, the mathematical model of maglev system is presented, and the force actuated by the electromagnet is formulated as [18]
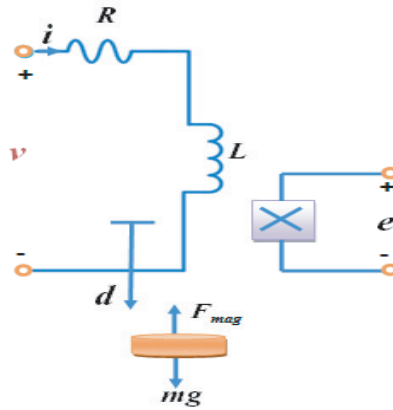
$$F_{mag} = C\frac{i(t)}{d^3} \tag{1}$$

Figure 2. Electromagnetic levitation system model.

where (t) denotes the current across the electromagnet, d the vertical position, and C a constant related to turn ratio and cross sectional area of the electromagnet. From a force balancing equation, we have

$$m\ddot{d} = mg - C\frac{i(t)}{d^3} \tag{2}$$

where m is the mass of the levitating magnet plus one-fourth of the mass of the acrylic plate and g the acceleration due to gravity.

In addition, an electrical relation of the voltage supply and the electromagnetic coil can be expressed by

$$v(t) = R \cdot i(t) + L\frac{di}{dt} \tag{3}$$

where R and L are the resistance and inductance of the electromagnet, respectively. Now consider the following perturbations with respect to the change of them

$$
\begin{aligned}
i(t) &= i_0 + \Delta i(t) \\
d(t) &= d_0 + \Delta d(t) \\
v(t) &= v_0 + \Delta v(t)
\end{aligned}
\tag{4}
$$

where v_o is the required equilibrium coil voltage to suspend the levitating plate at d_o.

Under this perturbation, the dynamics in Eqs. (2) and (3) around an operating point (i_0, d_0, v_0) can be linearized

$$m\ddot{\Delta}d = \left(\frac{3Ci_0}{d_0^4}\right)\Delta d - \left(\frac{C}{d_0^3}\right)\Delta i \tag{5}$$

$$\dot{\Delta}i = -\frac{R}{L}\Delta i - \frac{1}{L}\Delta v \tag{6}$$

where Δi, Δv, Δd are linearization of the system about the equilibrium point. After eliminating Δi in Eq. (6) and applying Laplace transforms, we obtain the transfer function from Δv to Δd given as

$$\frac{\Delta D(s)}{\Delta V(s)} = \frac{-\dfrac{gR}{v_0}}{(Ls + R)\left(s^2 - \dfrac{3Ci_0}{md_0^4}\right)} \tag{7}$$

where $\Delta V(s)$ and $\Delta D(s)$ denote the Laplace transforms of $\Delta v(t))$ and $\Delta d(t)$, respectively.

Hall sensor has an output voltage of the given form [19]

$$e(t) = \alpha + \frac{\beta}{d^2} + \gamma i(t) \tag{8}$$

where α, β, γ are constant sensor parameters. A linearization of Eq. (8) around $e(t) =_{e0} +\Delta e$ results in

$$\Delta e = -\frac{2\beta}{d_0^3}\Delta d + \gamma \Delta i \tag{9}$$

where Δe is the sensor voltage.

Applying Laplace transform to Eq. (9) and using $I(s) = \Delta V(s)/(Ls + R)$ from Eq. (3) and the representation in Eq. (7), we obtain a relation between the electromagnet voltage $\Delta V(s)$ and a sensor voltage perturbation $\Delta E(s)$ as follows;

$$\frac{\Delta E(s)}{\Delta V(s)} = \frac{\gamma\left(s^2 - \dfrac{3Ci_0}{md_0^4}\right) + \dfrac{2\beta RC}{md_0^6}}{(Ls + R)\left(s^2 - \dfrac{3Ci_0}{md_0^4}\right)} \tag{10}$$

Equation (10) can be represented also in the state space form after applying the second derivative of Eq. (5) and first derivative of Eq. (6). Thus, the state space representation of the linearized model of Equation (10) can be represented by followings:

$$\begin{bmatrix} \dot{x}_1 \\ \dot{x}_2 \\ \dot{x}_3 \end{bmatrix} = \begin{bmatrix} 0 & 1 & 0 \\ 3\dfrac{C}{m}\dfrac{i_0}{d_0^4} & 0 & -\dfrac{C}{m}\dfrac{1}{d_0^3} \\ 0 & 0 & -\dfrac{R}{L} \end{bmatrix} \begin{bmatrix} x_1 \\ x_2 \\ x_3 \end{bmatrix} + \begin{bmatrix} 0 \\ 0 \\ \dfrac{1}{L} \end{bmatrix} u \tag{11}$$

$$y = \begin{bmatrix} -2\dfrac{\beta}{d^3} & 0 & \gamma \end{bmatrix} \begin{bmatrix} x_1 \\ x_2 \\ x_3 \end{bmatrix} \tag{12}$$

The measured output system (y) can be obtained by simplified Equation (9), where $\Delta e = y$, $\Delta d = x_1$, and $\Delta i = x_3$).

Suppose that $x = [x_1 \ x_2 \ x_3] = [d \ \dot{d} \ i]$ is the state of the system, where d is the controlled output, $y = e$ the measured output, and $u = v$ the control input.

By substituting system parameters in Table 1 into Eq. (10),

$$G(s)H(s) = \frac{20.66s^2 + 61803}{s^3 + 132.5s^2 - 1471s - 194900} \tag{13}$$

The numerical values of the state space equations are given below

$$\begin{bmatrix} \dot{x}_1 \\ \dot{x}_2 \\ \dot{x}_3 \end{bmatrix} = \begin{bmatrix} 0 & 1 & 0 \\ 1471 & 0 & -9.81 \\ 0 & 0 & -133 \end{bmatrix} \begin{bmatrix} x_1 \\ x_2 \\ x_3 \end{bmatrix} + \begin{bmatrix} 0 \\ 0 \\ 66.66 \end{bmatrix} u \tag{14}$$

$$y = \begin{bmatrix} -144 & 0 & 0.31 \end{bmatrix} \begin{bmatrix} x_1 \\ x_2 \\ x_3 \end{bmatrix} \tag{15}$$

4. CONTROLLER DESIGN

This section deals with the development of PID based control and LQR controller for magnetic levitation system

4.1. Linear Quadratic Regulator (LQR) Controller

The Linear Quadratic Regulator (LQR) method is similar to Root Locus approach by inserting the closed loop poles of the system into the desired location [20]. The EMS linearization dynamic model is formulated by state space as below:

$$\dot{x}(t) = Ax(t) + Bu(t) \tag{16}$$
$$y(t) = Cx(t) + Du(t) \tag{17}$$

Table 1. Proposed system parameter.

	Parameter	Value	Unit
Sensor	β	5.64×10^{-4}	$\text{V} \cdot \text{m}^2$
	γ	0.31	V/A
	α	2.48	V
Operation point	i_0	1	A
	d_0	20	mm
Electromagnet	C	2.4×10^{-6}	$\text{kgm}^5/\text{s}^2\text{A}$
	R	2	Ω
	L	15×10^{-3}	H
	$m = M/4$	0.02985	kg

The $x(t)$ state can be measured, and the cost function of constructing controller can be minimized based on the formula below:

$$J(u) = \int\limits_0^{+\infty} \left(x^T(t) Q x(t) + u^T(t) R u(t) \right) dt \tag{18}$$

where Q and R values can be considered positive definite weighting matrices. For initial state condition, the variable $x(0)$ is considered as a steady state based on perturbation of the control system. The first term of the $J(u)$ function is considered as cost subject which is assigned to the energy intransient response.

The control signal $u(t)$ is considered as linearly proportional to the specified air gap. It is also proportional to the clearance of track boundary condition at desired operating point (i_o, z_o) in design stage.

Using the linear state feedback can be expressed by the equation below

$$u(t) = -[k_p (x_1(t) - z_{ref}) + k_v (x_2(t)) + k_a(x_3(t))] \tag{19}$$

where k_p is the steady error, k_v the control suspension damping, and k_a taken for all stability margins. The linear controller limitations are considered as the ability to suppress disturbances in the control loop. The calculated LQR gains are $[k_p = 32483, \; k_v = 90.4, \; k_a = -9.4]$.

4.2. PID Controller

The schematic diagram of PID controller is given in Figure 3. This control system is working based on the calculations of the error value, trying to reduce the error percentage by adjusting the controller parameters. The general form of this controller is formulated as below [20].

$$u(t) = K_p \left(e(t) + \frac{1}{T_i} \int\limits_0^t e(\tau) \, d\tau + T_d \frac{de(t)}{dt} \right) \tag{20}$$

where $u(t)$ denotes the control signal, K_p the proportional gain, T_i the integral time, T_d the derivative time, and $e(t)$ the difference between the reference point and the actual plant output. K_p, T_i and T_d are tuned for better control operation. By placing the closed loop poles at $P = [-132.45 \; 38.36 \; -28.36]$, the calculated PID gains are $[K_p = 10, \; K_i = 4, \; K_d = 0.2]$.

5. PROPOSED SYSTEM DESIGN AND HARDWARE CONTROL UNIT

In this section, the proposed method and hardware control unit parts are described as in Figure 4. The SIMLAB contains a set of input representations and output representations. The SIMLAB hardware
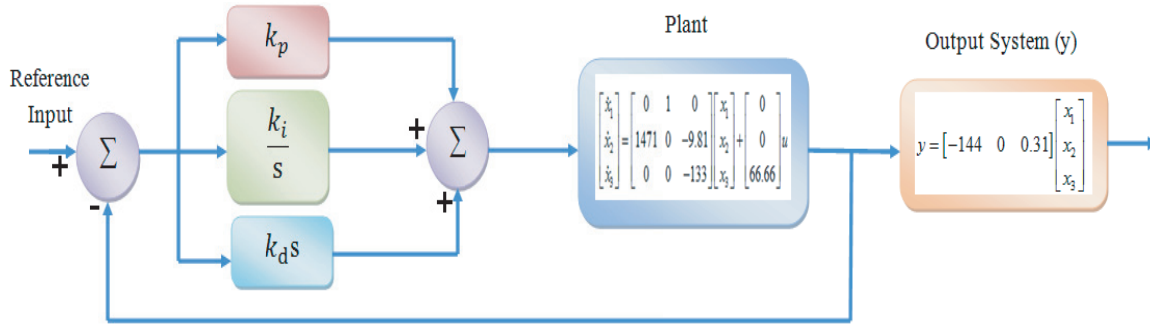
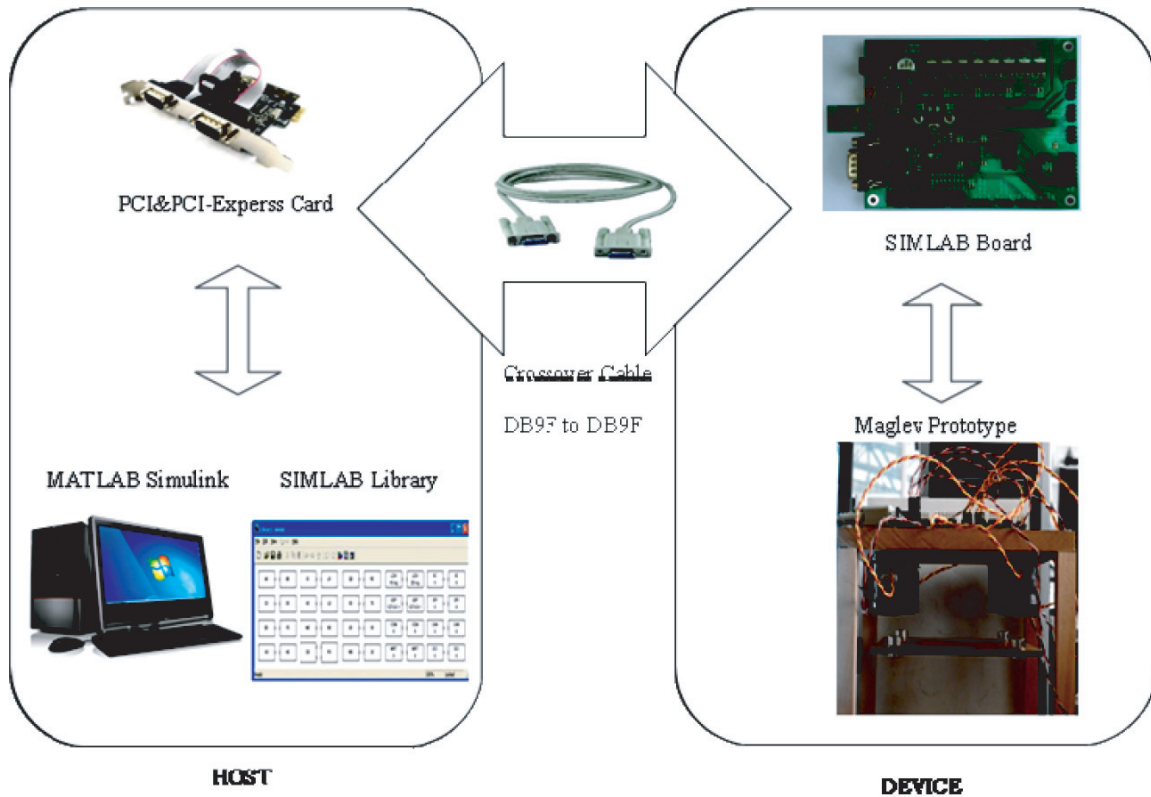**Figure 3.** Block diagram of PID controller.

Figure 4. Component of the maglev prototype system.

will be connected with both of the maglev prototype and the MATLAB Simulink which enables the system to control and operate. Proximity sensors are specific devices that enable the measurement of the air gap distance. There are many types of sensors such as laser, inductive, resistive, hall-effect and IR sensors. In the present system, the Hall-effect sensor is used to detect the distance of air gap. The sensor position in the present maglev system is at the bottom of the coil. The unique feature of this type of sensors encourages the researchers and producers to use it in many fields such as aircrafts, automobile and medical machines.

5.1. Experimental Results and Discussion

In this section, the experimental results are obtained based on different tests and parameters according to the proposed system design in Figure 5. The target is to investigate different types of response in

Figure 5. System implementation.

maglev system which represents the access point to maglev train. The results can be classified into two cases of test: signal representation test and load representation test as follows.

5.1.1. Results of Signal Representation Test

The first group of tests is the input signal representation. Two kinds of standard signals have been applied: Sine wave and Square wave. The input signal test was done with variation of different tuning parameters as follows.

I. Effect on One Point

The input of Sine wave signal was applied on one single point in the prototype maglev plate. The benefit of this test is to show the effect of sudden changes in one point on the maglev plane. The test signals were implemented with two types of control systems, PID and LQR, and the results are shown in Figures 6(a)–(b), respectively.

From the results indicated in Figure 6, it is noticed that the system performance is stable, and the system responses are perfect. Furthermore, the signal response that points x and x_3 respond based on the same input wave, while point x_1 responds oppositely. In this case, the system is able to convert the force reaction and dynamic moment in the load points (i.e., the discs) based on the load variation in each point of the plane. Moreover, the experimental results showed that LQR controller had optimum response and better stability than PID controller under the effect of the same input signal and parameters.

According to the findings obtained using input sine wave signal, another investigation was considered using a square wave signal. The simulation system was also carried out with the same assumption of the proposed system design. Here, it can be seen that the square wave tests indicate that the system response is also stable and offers acceptable response. The difference between square and sine wave results is the shape of changes in the signal in each point of the plate. The Sine wave signal revealed better response than the square wave because in the Sine wave, the signal has instantaneous change with time, and this can reduce the distortion. Also, the findings confirm that LQR offered better stability and response even though the input signal is different. The results are shown in Figures 7(a)–(b), respectively.
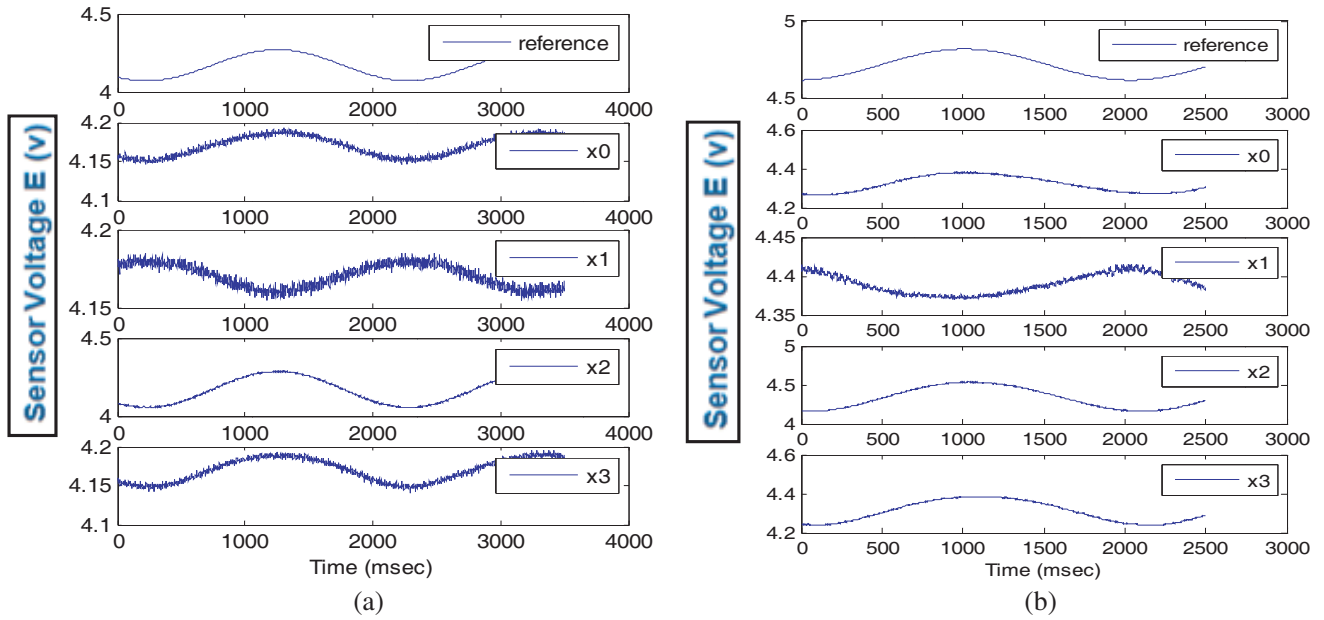
Figure 6. Sine wave signal applied on one single using (a) PID and (b) LQR controller.
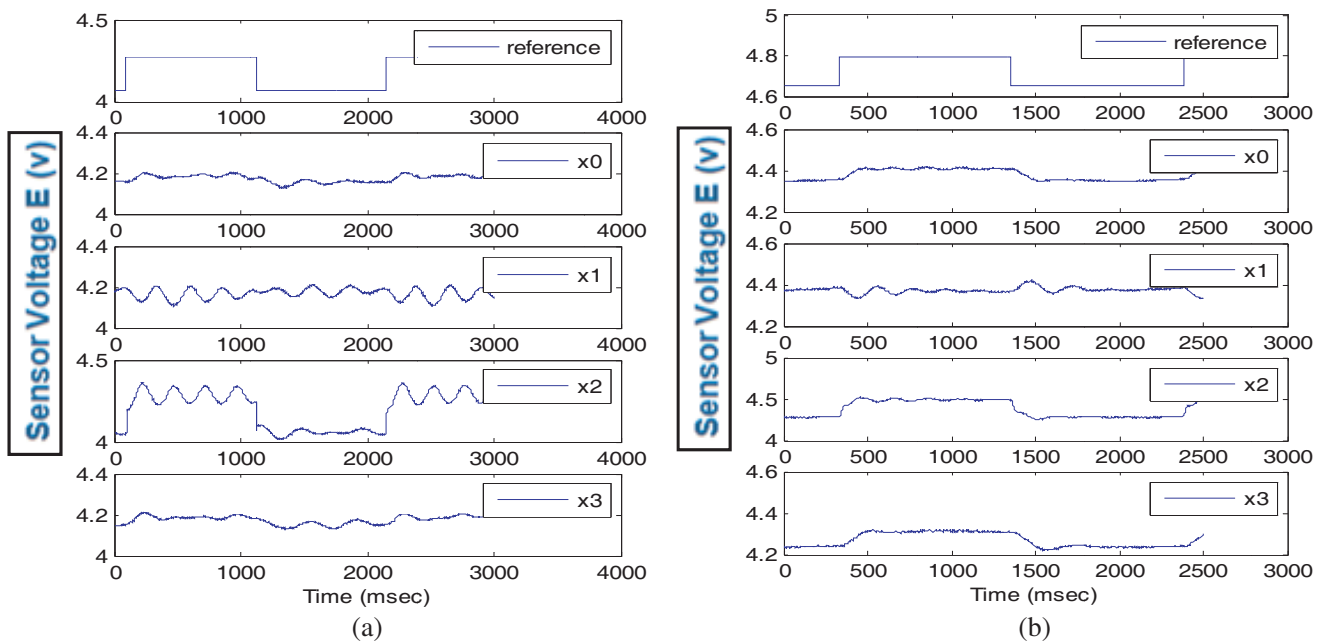

Figure 7. Square wave signal applied on one single using (a) PID and (b) LQR controller.

From all the results using (single point effect), it can be seen that Sine wave signal revealed better performance than square wave signal in both stability and response.

5.1.2. Results of Load Representation Test

In this test, the load impact on maglev system is considered. The applied load is equivalent to or mimics the real use of maglev train when it carries the humans and materials (the goods). This type of test includes two cases of load experiments. The first one is the one point load handling test. It represents a single load of 10 grams handled with one of the maglev system magnet discs. The second test is the
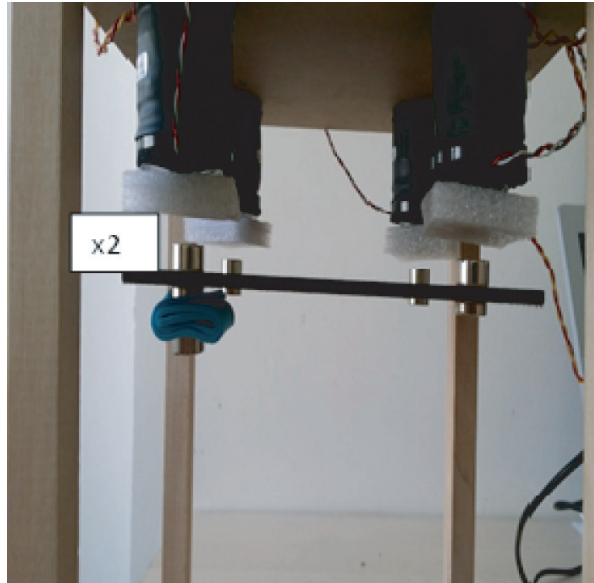
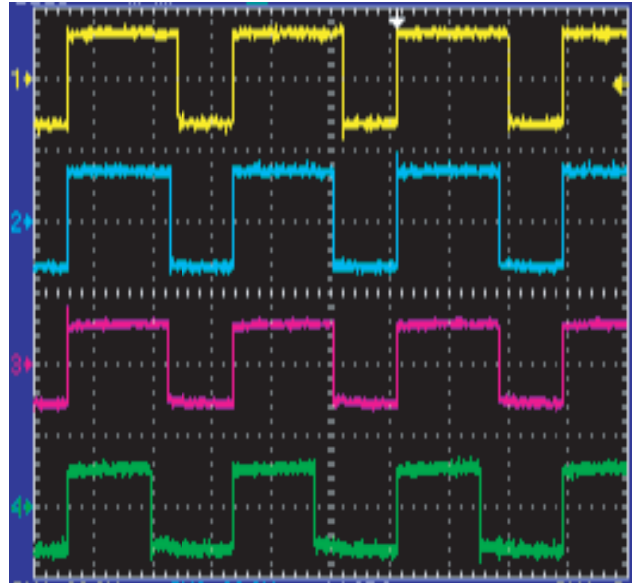**Figure 8.** Load test applied (one point).

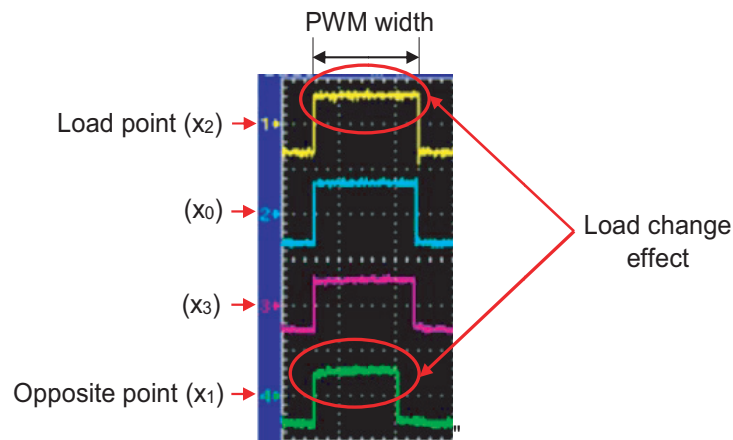**Figure 9.** PWM results of load test applied one single point.

Figure 10. PWM comparative of coil voltage response.

plane load of the maglev system plate which represents the whole system.

I. Case One: Effect on One Point

In this case, the input actual load of 10 grams is applied on one single point in the prototype maglev plate. The reason of applying this test is to investigate the effect of unbalance change of load in the plate based on one point of maglev plane. The test applied on point x_2 is as shown in Figure 8.

The load test is done with LQR control system, and the results are presented in Figure 9. The results indicate that the system is stable, and the system responds perfectly. It is clear from the pulse width modulation (PWM) results that the controller power supply of the present maglev system responds significantly as shown in Figure 10. It is seen that the average value of the voltage fed to the coils differs from point x_2 which represents the load input point and point x_1 which represents the opposite side point.

II. Case Two: Effect on Three Point (Plane)

In this case, the effect of load is applied on all plate points (magnet discs) in the maglev prototype. Figure 11 shows the suspended load on the system plate.
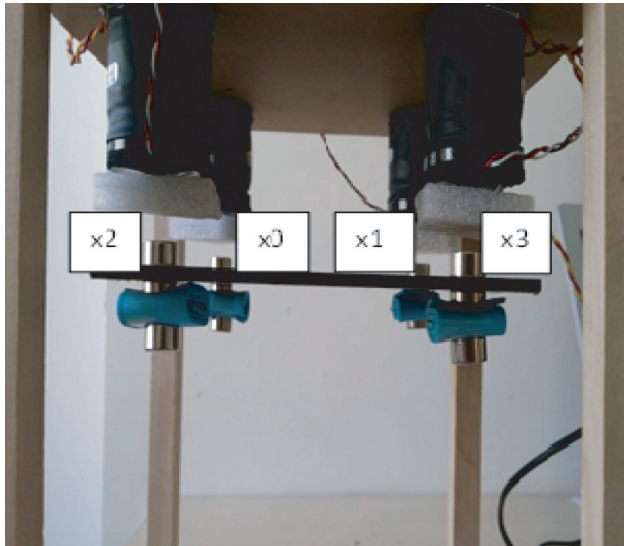
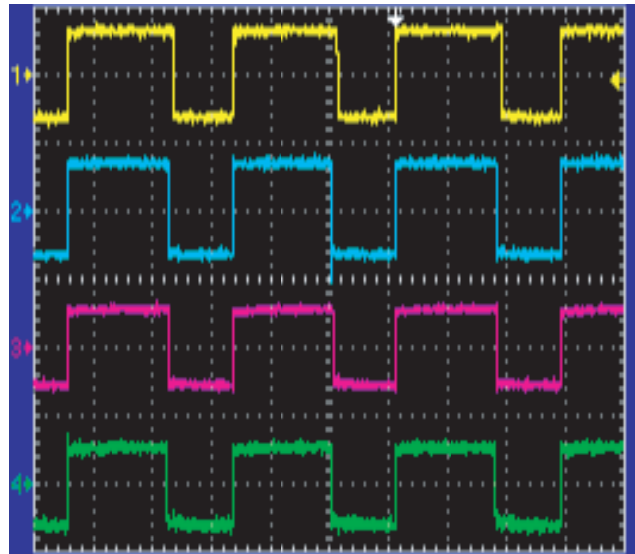**Figure 11.** Suspended load on the system plate.

Figure 12. PWM results of load applied on a plane.

The test load is applied using the LQR control system as presented before, as shown in Figure 12. From this result it can be observed that the system ability to deal with the force reaction and the dynamic moment in the load line is based on the load variation in four points of the plane.

It is clear from the pulse width modulation (PWM) results that the control power supply of the present maglev system responds significantly. Also, the system responds homogeneously, and all points respond based on the same input load at the same time of sequence. It means that the system is able to deal with the force reaction and the dynamic moment of the plane.

6. CONCLUSION

In this paper, an efficient technique of magnetic levitation system is proposed and successfully tested based on SIMLAB platform in real time operation. Furthermore, the proposed system was described mathematically and implemented practically under different tests and parameters. The present levitation system was implemented with modern controller which is LQR controller and compared with classical controller like PID controller under the same tuning parameters. Moreover, the proposed system has been examined under two tests: signal test and load test. The findings show that the LQR controller revealed a significant improvement in system performance. It was observed that LQR controller offered notable stability and better response than PID controller at the same input parameters.

REFERENCES

1. Ono, M., S. Koga, and H. Ohtsuki, "Japan's superconducting Maglev train," *IEEE Instrum. Meas. Mag.*, Vol. 5, No. 1, 9–15, 2002.
2. Chen, M.-Y., M.-J. Wang, and L.-C. Fu, "A novel dual-axis repulsive maglev guiding system with permanent magnet: Modeling and controller design," *IEEE/ASME Trans. Mechatron.*, Vol. 8, No. 1, 77–86, 2003.
3. De Boeij, J., M. Steinbuch, and H. Gutierrez, "Real-time control of the 3-DOFsled dynamics of a null-flux Maglev system with a passive sled," *IEEE Trans. Magn.*, Vol. 42, No. 5, 1604–1610, 2006.
4. Rote, D. and Y. Cai, "Review of dynamic stability of repulsive-force maglev suspension systems," *IEEE Trans. Magn.*, Vol. 38, No. 2, 1383–1390, 2002.

5. Banerjee, S., D. Prasad, and J. Pal, "Design, implementation, and testing of a single axis levitation system for the suspension of a platform," *ISA Trans.*, Vol. 46, No. 2, 239–246, 2007.

6. Lee, Y., J. Yang, and S. Shim, "A new model of magnetic force in magnetic levitation systems," *J. Electr. Eng. . . .*, Vol. 3, No. 4, 584–592, 2008.

7. Khemissi, Y., "Control using sliding mode of the magnetic suspension system," *International Journal of Electrical & Computer Sciences*, No. 3, 1–5, 2010.

8. Liu, C. and J. Zhang, "Design of second-order sliding mode controller for electromagnetic levitation grip used in CNC," *Proc. 2012 24th Chinese Control Decis. Conf. CCDC 2012*, Vol. 2, No. 1, 3282–3285, 2012.

9. Xing, F., B. Kou, C. Zhang, Y. Zhou, and L. Zhang, "Levitation force control of maglev permanent synchronous planar motor based on multivariable feedback linearization method," *2014 17th International Conference on Electrical Machines and Systems (ICEMS)*, 1318–1321, 2014.

10. Zhu, H., T. J. Teo, and C. K. Pang, "Design and modeling of a six-degree-of-freedom magnetically levitated positioner using square coils and 1-D Halbach arrays," *IEEE Trans. Ind. Electron.*, Vol. 64, No. 1, 440–450, 2017.

11. Vinodh Kumar, E. and J. Jerome, "LQR based optimal tuning of PID controller for trajectory tracking of magnetic levitation system," *Procedia Eng.*, Vol. 64, 254–264, 2013.

12. Hussein, B., N. Sulaiman, R. Raja Ahmad, M. Marhaban, and H. Ali, H_infinity controller design to control the single axis magnetic levitation system with parametric uncertainty," *J. Appl. Sci.*, Vol. 11, No. 1, 66–75, 2011.

13. Cho, J. and Y. Kim, "Design of levitation controller with optimal fuzzy PID controller for magnetic levitation system," *J. Korean Inst. Intell. Syst.*, Vol. 24, No. 3, 279–284, 2014.

14. Zhang, Y., Z. Zheng, J. Zhang, and L. Yin, "Research on PID controller in active magnetic levitation based on particle swarm optimization algorithm," *Open Automation & Control Systems Journal*, Vol. 7, No. 1, 1870–1874, 2015.

15. Uroš, S., A. Sarjaš, A. Chowdhury, and R. Svečko, "Improved adaptive fuzzy back stepping control of a magnetic levitation system based on symbiotic organism search," *Applied Soft Computing*, Vol. 56, 19–33, 2017.

16. Hong, D.-K., B.-C. Woo, D.-H. Koo, and K.-C. Lee, "Electromagnet weight reduction in a magnetic levitation system for contactless delivery applications," *Sensors*, Vol. 10, 6718–6729, 2010.

17. Li, J.-H. and J.-S. Chiou, "Digital control analysis and design of a field-sensed magnetic suspension system," *Sensors*, Vol. 15, 6174–6195, 2015.

18. Cheng, D. K., *Field and Wave Electromagnetics*, Addison-Wesley, MA, 1983.

19. Smaili, A. and F. Mrad, *Applied Mechatronics*, Oxford, MA, 2008.

20. Unni, A. C., A. S. Junghare, V. Mohan, W. Ongsakul, and E. Fos, "PID, fuzzy and LQR controllers for magnetic levitation system," Vol. 0, No. September, 14–16, 2016.